Optimized Maximum Power Point Tracker for Fast-Changing Environmental Conditions

Dezso Sera, *Student Member, IEEE*, Remus Teodorescu, *Senior Member, IEEE*, Jochen Hantschel, and Michael Knoll

***Abstract*—This paper presents a high-performance maximum power point tracker (MPPT) optimized for fast cloudy conditions, e.g., rapidly changing irradiation on the photovoltaic panels. The rapidly changing conditions are tracked by an optimized hill–climbing MPPT method called dP-P&O. This algorithm separates the effects of the irradiation change from the effect of the tracker's perturbation and uses this information to optimize the tracking according to the irradiation change. The knowledge of the direction of the irradiation change enables the MPPT to use different optimized tracking schemes for the different cases of increasing, decreasing, or steady irradiance. When the irradiance is changing rapidly this strategy leads to faster and better tracking, while in steady-state conditions it leads to lower oscillations around the MPP. The simulations and experimental results show that the proposed dP-P&O MPPT provides a quick and accurate tracking even in very fast changing environmental conditions.**

***Index Terms*—Fast-changing irradiation, maximum power point tracking, photovoltaic, solar.**

I. INTRODUCTION

THE worldwide-installed photovoltaic (PV) power capacity today shows a nearly exponential increase, which is mostly dominated by grid-connected applications [1]. In these applications, the typical goal is to extract the maximum possible power from the PV plant during the entire time of operation; thereby, these systems need a maximum power point tracker (MPPT), which sets the system working point to the optimum, following the weather (i.e., solar irradiance and temperature) conditions. There are many MPPT strategies that are available [2]–[10] for different converter topologies, which provide high performance tracking during "nice" weather conditions, i.e., at strong and stable solar irradiation and no partial shadowing. These trackers are satisfactory if the PV system is installed at a place where the possibility of clouds and partial shading is very low. However, in many cases, when the PV system is installed in an urban area, partial shadowing by the neighboring buildings is sometimes inevitable [11]. Similarly, on places where the moving clouds are very often present on the sky, for example, Northern Europe, the irradiation can show fast changes even though the average value is fairly high. In these cases, if the MPPT is not able to detect the partial shadowing and if is not able to react quickly to the fast irradiation changes, the PV system capacity will not be optimally used.

Manuscript received October 31, 2007; revised March 27, 2008.

D. Sera is with the Institute of Energy Technology, Aalborg University, 9220 Aalborg East, Denmark (e-mail: des@iet.aau.dk).

R. Teodorescu is with the Power Electronics Section, Green Power Laboratory, Institute of Energy Technology, Aalborg University, 9220 Aalborg East, Denmark (e-mail: ret@iet.aau.dk).

J. Hantschel is with the REFU-Elektronik GmbH, 72555 Metzingen, Germany (e-mail: jochen.hantschel@refu-elektronik.de).

M. Knoll was with the REFU-Elektonik GmbH, 72555 Metzingen, Germany. He is now with Daimler AG, 70546 Stuttgart, Germany (e-mail: ferchau.knoll@daimler.com).

Color versions of one or more of the figures in this paper are available online at http://ieeexplore.ieee.org.

Digital Object Identifier 10.1109/TIE.2008.924036

II. MPPTs IN RAPIDLY CHANGING CONDITIONS

As it was mentioned in Section I, an MPPT algorithm that provides high-performance tracking in steady-state conditions can easily be found. A very popular hill-climbing method is the perturb and observe (P&O) [2], [12], [13] tracker, which has some important advantages as simplicity, applicability to almost any PV system configuration, and good performance in steady-state operation. However, as with most of the hill-climbing methods, there is a tradeoff between the accuracy and speed of the tracking.

A. dP-P&O Method

The dP-P&O MPPT method [14] is an improvement of the classical P&O in the sense that it can prevent itself from tracking in the wrong direction during rapidly changing irradiance, which is a well-known drawback of the classical P&O algorithm.

The dP-P&O determines the correct tracking direction by performing an additional measurement in the middle of the MPPT sampling period, as shown in Fig. 2. As it can be seen in the figure, the change in power between P_x and P_{k+1} only reflects the change in power due to the environmental changes, as no action has been made by the MPPT. The difference between P_x and P_k contains the change in power caused by the perturbation of the MPPT plus the irradiation change. Thereby, assuming that the rate of change in the irradiation is constant over one sampling period of the MPPT, the dP that is purely caused by the MPPT command can be calculated as follows:

$$\begin{aligned} dP &= dP_1 - dP_2 = (P_x - P_k) - (P_{k+1} - P_x) \\ &= 2P_x - P_{k+1} - P_k. \end{aligned} \tag{1}$$

The resulting dP reflects the changes due to the perturbation of the MPPT method. The flowchart of the dP-P&O can be seen in Fig. 1. Equation (1) represents a small extra computational load compared to the classical P&O method, where, in order to determine the next perturbation direction, a difference between two consecutive measurements of power is used (Fig. 2). In case of dP-P&O, an extra measurement needs to be taken;

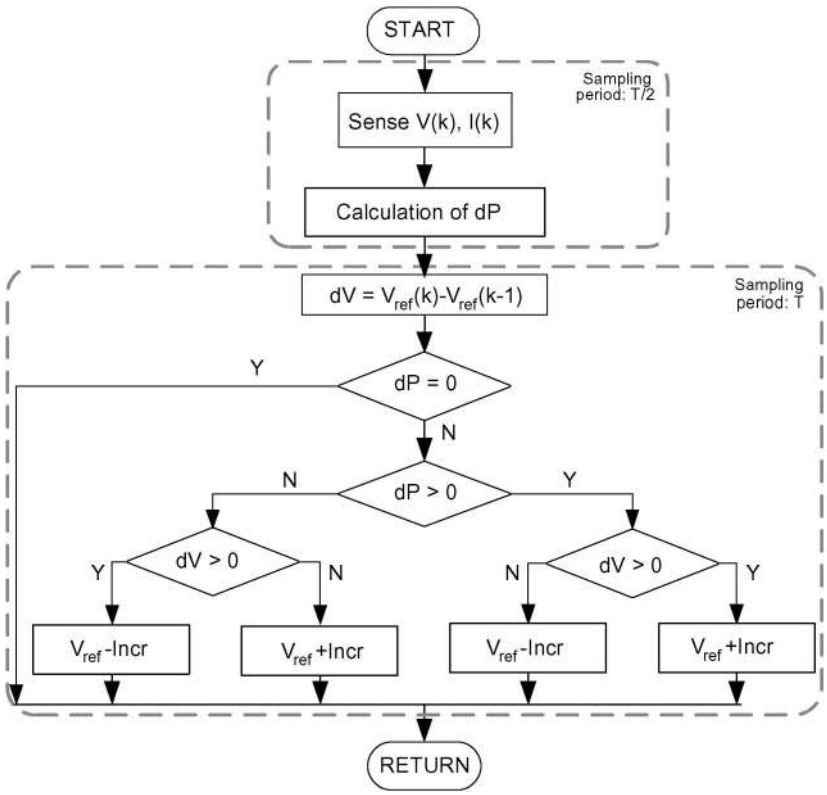

Fig. 1. Flowchart of the dP-P&O algorithm.

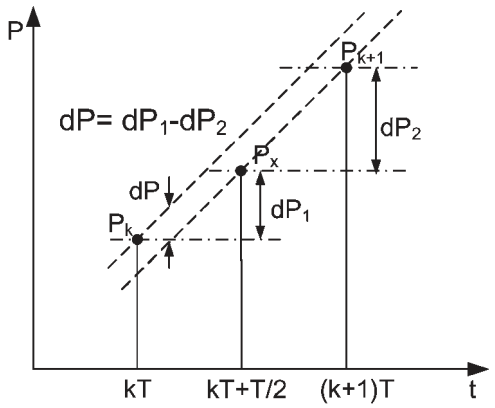

Fig. 2. Measurement of the power between two MPPT sampling instances.

however, this does not require a new sampling of the measured PV voltage and current, as they are sampled with high frequency for the dc voltage controller and power feedforward (see Fig. 4).

Determining the dP allows tracking in the correct direction during irradiation changes. However, in order to track very fast changes of irradiation, the voltage perturbation step has to be increased. This would lead to oscillations around the MPP in steady-state conditions, degrading the overall performance. To overcome this drawback, the information regarding the change of output power due to external conditions dP_2 is used. From the value of dP_2, it can be determined if the irradiation is stable, increasing, or decreasing. This information allows the use of an optimized tracking strategy for the different cases. The flowchart of this method is shown in Fig. 3.

In Fig. 3, the symbols have the following meanings:

1) ThN—negative threshold for dP;
2) ThP—positive threshold for dP.

In Fig. 3, if the change in power due to irradiation ($|dP_2|$) is smaller than the change of power due to the MPPT perturbation ($|dP|$), it is considered to be a slowly changing condition and the system will use the basic dP-P&O algorithm with small increment values to reduce oscillations around the MPP.

B. Optimized dP-P&O During Rapidly Changing Irradiation

The inverter control system considered when examining the optimized dP-P&O MPPT is shown in Fig. 4.

In Fig. 4, the MPPT gives the voltage reference to the dc voltage controller, whose output will serve as the reference for the grid current peak value. The dc voltage controller is a proportional integrator, whereas the grid current controller is considered ideal as well as the inverter.

If a fast rise of irradiation was detected by dP_2 in Fig. 3, it means that the MPPT should increase the PV array reference voltage in order to follow the irradiation change. Thereby, in this situation, the MPPT switching strategy is in favor of increasing the voltage reference. $V_{\rm dc}$ref in Fig. 4 is decreased only when the voltage was increased in the previous MPPT sampling instance, and it caused a reduction of power $dP <$ ThN. A negative threshold value ThN has been applied in order to avoid unnecessary switching around the MPP. If—due to the action of the MPPT in the last sampling period—dP becomes negative, the MPPT holds the voltage reference at the same level for one sampling period instead of decreasing it, unless

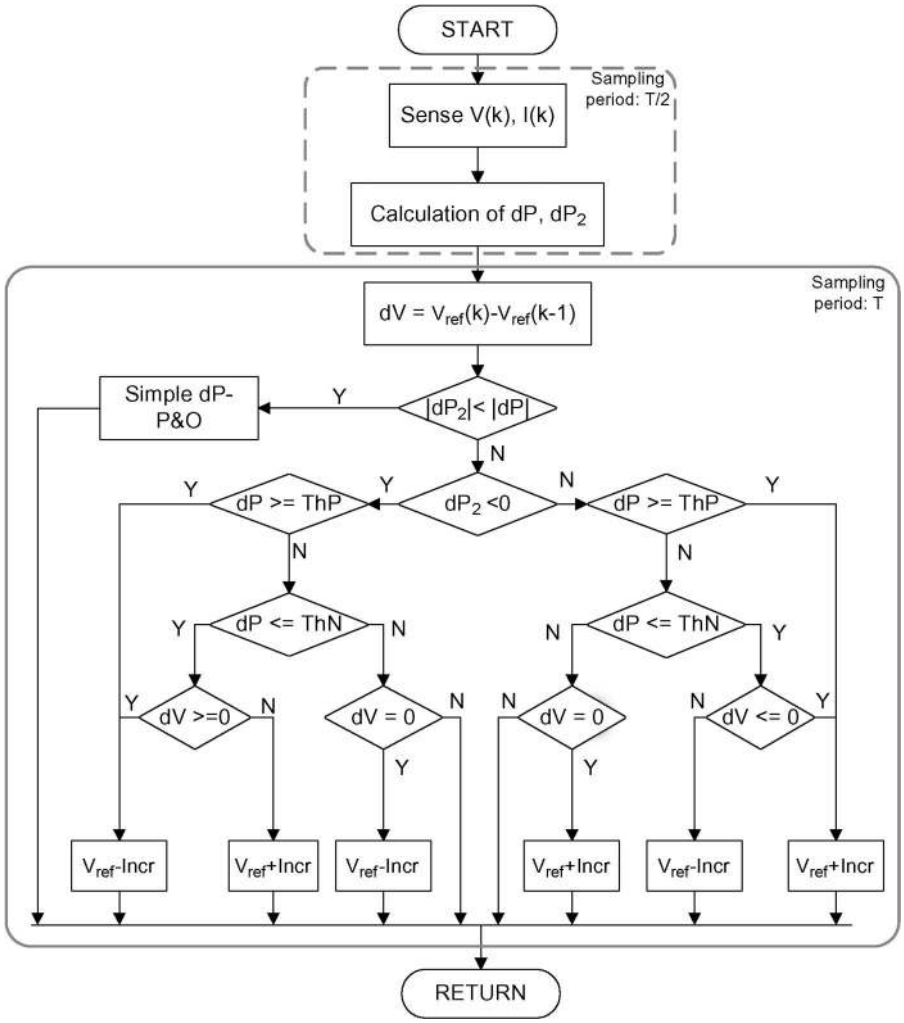

Fig. 3. Flowchart of the dP-P&O method with optimized tracking.

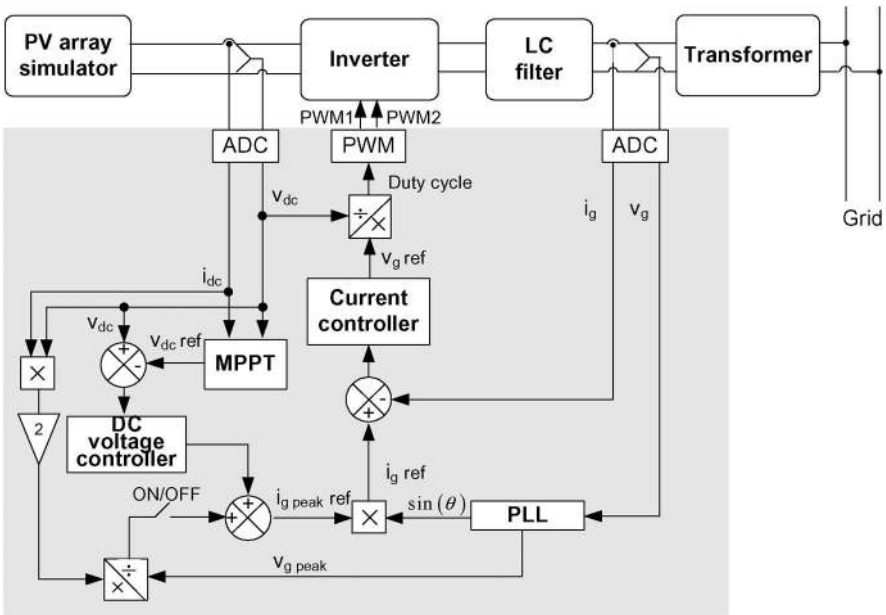

Fig. 4. Single phase MPPT and current control structure for green power inverter.

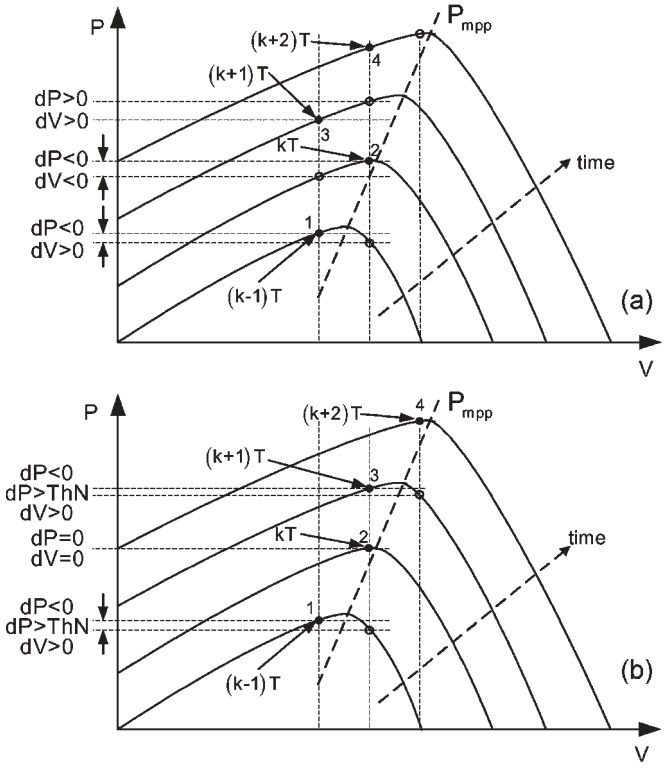

Fig. 5. Movement of the operating point of the PV system on the P–V characteristic (a) with the basic dP-P&O tracking method and (b) with the optimized tracking.

the caused decrease of power became larger than the threshold ($|dP| > |\text{ThN}|$). The flowchart in Fig. 3 assumes that the MPP voltage increases with irradiance, which is valid in most of the cases. However, in some cases, due to the panel series resistance at high irradiation levels, the MPP voltage could decrease with irradiation [15].

C. Determination of the Threshold Values

A theoretical analysis regarding the optimal choice of the main parameters (sampling frequency and perturbation size) of the P&O method, which is also valid for the dP-P&O, can be found in [16].

The threshold ThP has been chosen to be zero. This is because if the last perturbation had a positive effect on the output power, regardless of the size of the change, the MPPT should continue the perturbation in the same direction. A nonzero ThP would introduce a stationary error in the tracking by stopping the perturbation when the working point is approaching the MPP. On the other hand, when choosing the negative threshold ThN, the goal is to avoid unnecessary switching when the MPPT is closely following the changing MPP in varying irradiation, as it is shown in Fig. 5. If |ThN| is chosen to be too large, it would allow the working point to move away too far from the MPP, decreasing the MPPT efficiency. On the other hand, if |ThN| is too small, it will result in unnecessary switching around the MPP, also causing additional losses. In order to obtain the value of ThN, the change of power ΔP_I due to one voltage increment in the vicinity of MPP should be determined first, which requires a model of the used PV system. For the present purpose, a simple model is sufficient.

The current–voltage relationship of a PV panel using an ideal single-diode model can be described as follows:

$$I = I_{\text{sc}} - I_0 \left(e^{\frac{V}{n_s V_t}} - 1 \right) \tag{2}$$

where I_{sc} is the panel short-circuit current, I_0 is the dark saturation current, and V_t is the cell's thermal voltage. I_{sc} is given in the panel data sheet, whereas I_0 and V_t can be calculated by using the data sheet values and the panel basic equations or by measurements [17]–[19].

From (2), the panel voltage as a function of current can be expressed as follows:

$$V = n_s V_t \ln \left(\frac{I_{\text{sc}} - I}{I_0} \right). \tag{3}$$

If the PV system current is perturbed by a small dI, from (3)

$$V' = n_s V_t \ln \left(\frac{I_{\text{sc}} - I - dI}{I_0} \right). \tag{4}$$

From (3) and (4), the change of voltage caused by the small current perturbation can be calculated as follows:

$$\begin{aligned} dV_I &= V' - V \\ &= n_s V_t \left(\ln \left(\frac{I_{\text{sc}} - I - dI}{I_0} \right) - \ln \left(\frac{I_{\text{sc}} - I}{I_0} \right) \right) \end{aligned} \tag{5}$$

$$dV_I = n_s V_t \ln \left(\frac{I_{\text{sc}} - I - dI}{I_{\text{sc}} - I} \right). \tag{6}$$

By solving (6) for dI, the effect of a small voltage perturbation on the array current can be obtained as follows:

$$dI_V = (I_{\text{sc}} - I) \left(1 - e^{\frac{dV}{n_s V_t}} \right). \tag{7}$$

The general expression of the power change due to a small voltage perturbation has the form

$$dP_V = dV I + dI_V V + dI_V dV. \tag{8}$$

By inserting (7) into (8), the PV power change due to a small voltage perturbation at an arbitrary point of the V–I characteristic can be estimated.

If one replaces the term dV in the aforementioned equation with Incr, it will result in the variation of power due to one perturbation of the MPPT.

Obviously, (8) depends on the actual irradiation conditions and the instantaneous working point of the system on the V–I characteristic. It is well known that, at a given irradiation intensity

$$\left. \frac{\partial P}{\partial V} \right|_{\text{MPP}} = 0. \tag{9}$$

From (9), the change of power due to a small ΔV is the minimum in the vicinity of the MPP

$$\left|\frac{\Delta P}{\Delta V}\right|_{\mathrm{MPP}} \leq \left|\frac{\Delta P}{\Delta V}\right|_{\substack{V\neq V_{\mathrm{MPP}}\\ I\neq I_{\mathrm{MPP}}}}. \tag{10}$$

The calculation of the threshold values are based on (8), where the actual working point on the I–V characteristic is considered to be $V = V_{\mathrm{MPP}} \pm \mathrm{Incr}$, with a perturbation that moves the working point away from MPP.

III. Simulation Results

The inverter-control structure shown in Fig. 4 has been implemented in Simulink in order to verify and compare the behavior of the optimized dP-P&O to the basic dP-P&O. The considered system parameters are described in the following. The PV array consists of three parallel strings, each containing 16 series-connected BPMSX120 PV panels with the following data sheet parameters:

1) $I_{\mathrm{sc}} = 3.87$ A—short-circuit current in STC[1];
2) $V_{\mathrm{OC}} = 42.1$ V—open-circuit voltage in STC;
3) $V_{\mathrm{MPP}} = 33.7$ V—voltage at the MPP in STC;
4) $I_{\mathrm{MPP}} = 3.56$ A—current at the MPP in STC;
5) $P_{\mathrm{MPP}} = 120$ W—power at the MPP in STC.

Considering that each string contains 16 panels with the aforementioned parameters, the rated MPP voltage of the system results as $V_{\mathrm{rated}} = 16 \times 33.7 = 539$ V. The maximum power of the entire plant results as $P_{\mathrm{rated}} = 3 \times 16 \times 120 = 5760$ W. The rated current of the system is $I_{\mathrm{rated}} = 3 \times 3.56 = 10.68$ A. The model of the PV plant is using the detailed single-diode model, considering the full characteristic of the cells, where the reverse characteristic equations were implemented according to [20]. The inverter and the grid current controller are considered ideal; they are modeled by an ideal current source and a two-sample delay, respectively. The LC filter and grid impedance have been modeled by using the PLECS toolbox, with values of $L_f = 1.7$ mH and $C_f = 4.3$ μF for the LC filter and $L_g = 50$ μH and $R_g = 0.2$ Ω for the grid impedance. The minimum system voltage allowed is $V_{\mathrm{sys\,min}} = 150$ V.

In order to visualize and compare the behavior of the initial and optimized dP-P&O algorithms, they have been simulated in the following two different MPPT configurations: 1) when the MPPT provides the dc current reference (Figs. 6 and 7) and 2) when the MPPT provides the dc voltage reference (Figs. 8 and 9). In the following, the simulation results for these two cases will be presented.

A. Comparison of the MPPT Algorithms With Current Reference as Output

In order to facilitate the comparison of the basic and optimized dP-P&O, the same current increment values were used

[1]Standard test conditions—The testing conditions to measure photovoltaic cell or module nominal output power. Irradiance level is 1000 W/m^2, with the reference air mass of 1.5 solar spectral irradiance distribution and cell or module junction temperature of 25 °C.

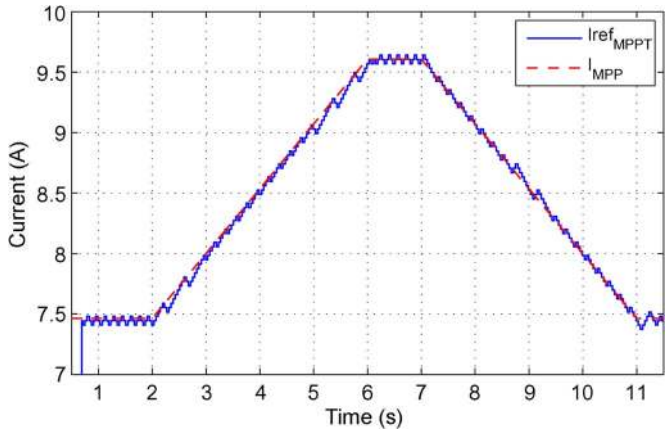

Fig. 6. Current references of the basic dP-P&O algorithm and the ideal MPP current during rapidly changing irradiation. It can be seen that the tracker "turns back" when it crosses the MPP current. The trapezoidal irradiation profile starts at 2 s on the time axis, reaches the maximum at 6 s, and returns to the initial level at 11 s.

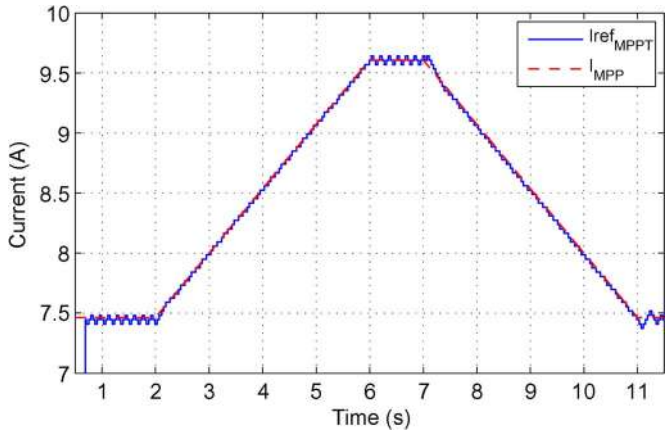

Fig. 7. Current references of the optimized dP-P&O algorithm and the ideal MPP current during rapidly changing irradiation. The tracker does not decrease the current reference when it reaches the MPPT current but waits for one MPPT period without perturbation instead.

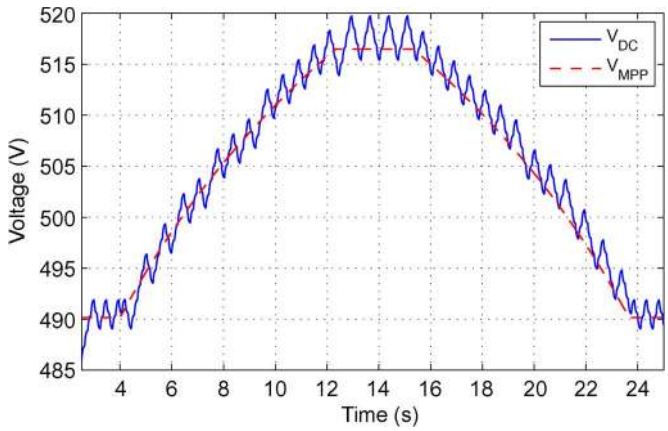

Fig. 8. PV system voltage and ideal MPP voltage during a trapezoidal irradiation profile. It can be seen that the dc voltage oscillates around the optimum value during the irradiation slope. The ramp starts at 4 s on the time axis from 250 W/m^2, reaches its maximum (500 W/m^2) at 12.5 s, and arrives back at its initial value at 24 s.

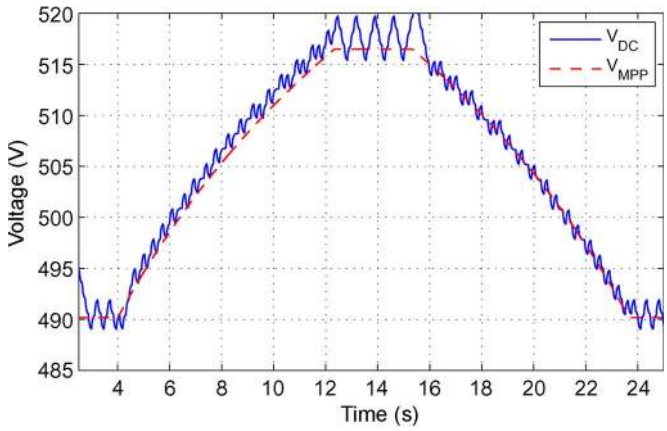

Fig. 9. PV system voltage and ideal MPP voltage during a trapezoidal irradiation profile. It can be seen that the dc voltage ripple is considerably decreased during the ramp.

for both strategies: $\text{Incr}_{\min} = 12$ mA for steady-state conditions and $\text{Incr} = 3 \times 12$ mA for rapidly changing conditions. The MPPT sampling frequency is, in both cases, $f_{\text{MPPT}} = 25$ Hz.

In order to verify the effect of rapidly changing irradiation conditions, an irradiation ramp change was used. This irradiation change starts from 700 W/m^2, stops at 900 W/m^2, waits at this level for 1 s, and decreases again back to 700 W/m^2 with a constant slope. A 4-s period for the increasing and decreasing ramps was selected. The aforementioned values were selected in order to shorten the simulation time; the focus was put on the visualization of the different tracking behaviors of the initial and optimized dP-P&O algorithms. One should note that, in case the MPPT provides the dc current reference instead of the dc voltage, it needs higher dynamics in order to be able to follow the increasing irradiance, which is due to the linear dependence of MPP current with irradiance, as opposed to the case with the MPP voltage logarithmic dependence.

B. Comparison of the MPPT Algorithms With Voltage Reference as Output

In the present section, the behaviors of the basic and optimized dP-P&O trackers with dc voltage reference (identical to the block scheme in Fig. 4) are simulated and compared. As this configuration has been implemented on the experimental setup, the simulation settings follow the practical case. Accordingly, a voltage increment of $\text{Incr} = 1$ V and an MPPT sampling rate of $f_{\text{MPPT}} = 8.33$ Hz (every sixth grid voltage period) are used, both in rapidly changing irradiation and steady-state conditions. An irradiation ramp starts from 250 W/m^2, stops at 500 W/m^2, waits at this level for 5 s, and again decreases back to 250 W/m^2 with a constant slope. The slope of the irradiation was chosen to be 30 W/m^2/s, which corresponds to 8.3 s as the duration of the increasing and decreasing ramps. The aforementioned values were selected in order to shorten the simulation time; the focus was put on the visualization of the different tracking behavior of the initial and optimized dP-P&O algorithms. The relatively low irradiation values were chosen in order to accentuate the effect of irradiation change on the PV system MPP voltage.

IV. Experimental Tests and Results

Both the traditional and improved methods were implemented and experimentally tested on an industrial PV inverter, which was manufactured by REFU Elektronik GmbH, Germany. The laboratory setup, using a control system as shown in Fig. 4, consists of the following main components.

A PV simulator, which is built of two programmable series-connected Delta Elektronika SM300-10 dc power supplies having Vmax $= 300$ V and Imax $= 10$ A, was used. Their output voltages were controlled in real time by a DS1103 dSpace system according to a PV model of a PV array. The model is based on a number of series-/parallel-connected BP-MSX120 PV panels where the input parameters are the maximum power in STC (P_{MP}), the voltage at the $P_{\text{MP}}(V_{\text{MP}})$, and the solar irradiation intensity.

The equations on which the model is based are shown as follows:

$$V = n_{\text{ps}} V_{\text{OC}} + n_{\text{ps}} \cdot n_s \cdot V_t \ln\left(1 - \frac{I}{I_{\text{sc,STC}} \cdot \frac{G}{1000}}\right)$$
$$V_{\text{OC}} = n_s V_t \ln\left(\frac{1 + I_{\text{sc,STC}} \cdot \frac{G}{1000}}{I_0}\right) \quad (11)$$

where

n_{ps}	number of panels connected in series;
n_s	number of cells in one panel;
V_t	thermal voltage (V);
$I_{\text{sc,STC}}$	short-circuit current at STC (A);
G	irradiation (W/m^2).

The output of the PV simulator is connected to the solar inverter manufactured by REFU Elektronik GmbH, Germany. The rated power of the PV inverter is 15 kW with a 50-Hz 400-V three-phase output and dc input voltage range of 150–800 V.

As the used solar inverter is a newly developed product by REFU Electronik, not all the technical parameters are available, only the ones relevant for MPPT operation. Thereby, the current control loop has been considered ideal from the MPPT point of view. The inverter has a dc link capacitor value of $C_{\text{dc}} = 4$ mF, and the system sampling frequency, which is identical to the switching frequency, is $f_{\text{sw}} = 16$ kHz. The sampling of the measured signals has a resolution of 12 b. The PV inverter real-time control is running on a Motorola PowerPC 400-MHz processor.

Due to the three-phase configuration and the large value of the dc link capacitor, the effects of power oscillations at double grid frequency on the dc link voltage have been neglected.

The MPPT structure of the solar converter corresponds to the one shown in Fig. 4. The MPPT dc voltage increment and perturbation frequency has been chosen identical for all three considered tests: the classic P&O (Fig. 10), the dP-P&O, as well as for the improved dP-P&O; these settings correspond to those described in Section III-B: $\text{Incr} = 1$ V and MPPT sampling rate $f_{\text{MPPT}} = 8.33$ Hz.

In order to test the MPP tracker behaviors in dynamic conditions, a linear irradiation ramp was used. The ramp starts

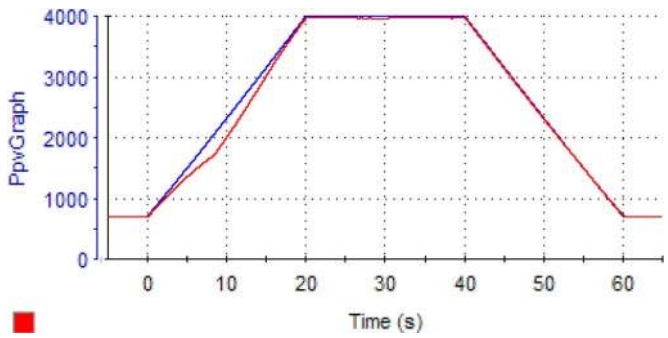

Fig. 10. Experimental measurement of the (red signal) PV array power during a trapezoidal irradiation profile, using the classical P&O MPPT method, compared to the (blue signal) ideal MPP power.

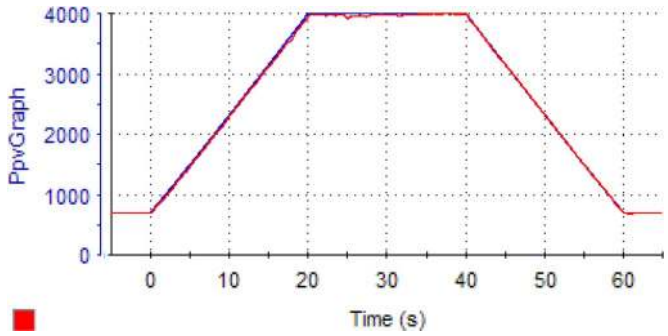

Fig. 11. Experimental measurement of the (red signal) PV array power (W) during a trapezoidal irradiation profile, using the dP-P&O MPPT method, compared to the (blue signal) ideal MPP power.

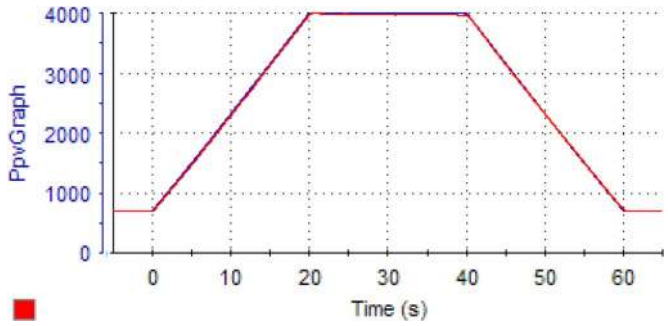

Fig. 12. Experimental measurement of the (red signal) PV array power (W) during a trapezoidal irradiation profile, using the optimized dP-P&O MPPT method, compared to the (blue signal) ideal MPP power.

at 5 s on the time axis from 200 W/m^2, reaches its maximum (1000 W/m^2) at 20 s, and arrives back to its initial value at 60 s.

In the following, the experimental results using the previously described setup will be presented.

It can be seen in Figs. 11 and 12 as well as in Figs. 13 and 14 that the optimized dP-P&O algorithm performs slightly better than the initial one. The relatively small difference in their performance is due to two main factors: 1) the noisy measurement environment, which is present in most applications and 2) the characteristic of the controlled dc voltage sources used as PV simulators. The sources have output capacitors for the reduction of voltage ripples, which inherently reduces

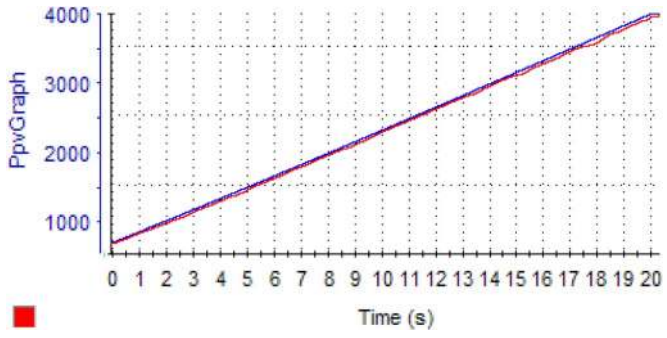

Fig. 13. Experimental measurement of the (red signal) PV array power (W) during a trapezoidal irradiation profile, using the dP-P&O MPPT method, compared to the (blue signal) ideal MPP power, which is zoomed on the increasing ramp.

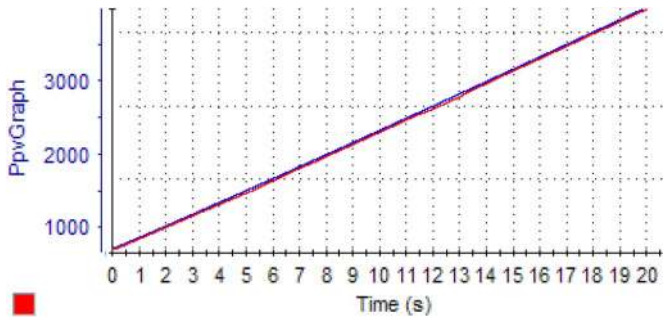

Fig. 14. Experimental measurement of the (red signal) PV array power (W) during a trapezoidal irradiation profile, using the optimized dP-P&O MPPT method, compared to the (blue signal) ideal MPP power, which is zoomed on the increasing ramp.

their control bandwidth. Thereby, the PV simulator cannot be considered identical to a real PV system in terms of voltage controllability and response time. This means that, around MPP, where a voltage perturbation creates a relatively small change of power [see (10)], the simulator has difficulties in adjusting the voltage accordingly. This results in larger voltage oscillations of the MPP tracker around the MPP than in the case of a real PV system, without decreasing the output power.

However, the considered MPPT algorithms are tracking the power and not the voltage; therefore, they are able to keep the output power close to the optimum (maximum) value in both cases. Nevertheless, an increase of efficiency in favor of the optimized dP-P&O can be seen when looking at the zoom of the increasing ramp of the power in Figs. 13 and 14. This can also be seen in the efficiency plots in Figs. 16 and 17.

Due to the facts considered previously and in order to show the real power tracking capabilities of the algorithms, they have been assessed based on comparing the inverter input power to the ideal MPP given by the model.

The instantaneous efficiencies corresponding to the traditional dP-P&O method can be seen in Fig. 15, whereas the basic and optimized dP-P&O algorithms are shown in Figs. 16 and 17, respectively. It can be seen that the average efficiency of the optimized dP-P&O during the entire test period is approximately 99.4%, which is about approximately 0.4% higher compared to the basic dP-P&O. It can also be noted that the efficiency in Fig. 17 shows less variation when compared to the basic dP-P&O efficiency plot.

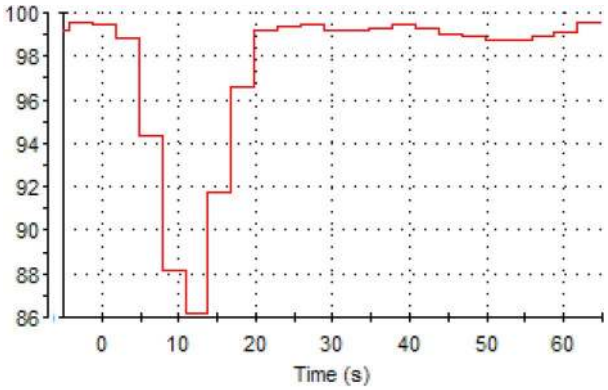

Fig. 15. Experimental measurement of the instantaneous MPPT efficiency (in percentage and averaged over 3 s) of the classical P&O algorithm.

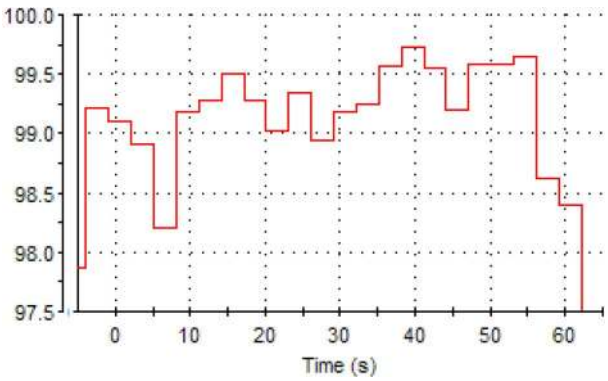

Fig. 16. Experimental measurement of the instantaneous MPPT efficiency (in percentage and averaged over 3 s) of the basic dP-P&O algorithm during the trapezoidal irradiation profile.

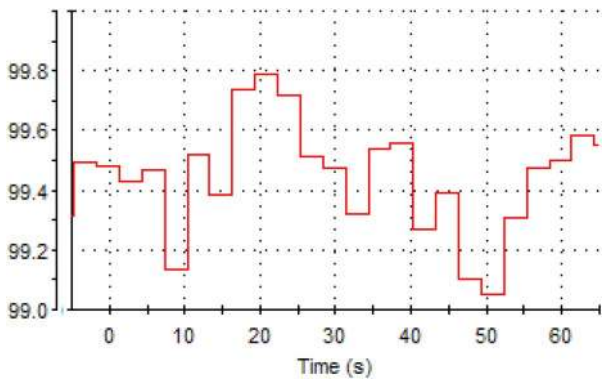

Fig. 17. Experimental measurement of the instantaneous MPPT efficiency (averaged over 3 s) of the optimized dP-P&O algorithm.

V. Conclusion

In this paper, a fast MPPT algorithm for rapid irradiation changes has been presented. The method is using an additional measurement of power inside the MPPT algorithm without perturbation and uses this information to separate the effects of the environment from the tracker's perturbations. Furthermore, by identifying the environmental changes, it allows the use of optimized tracking for different operational states: stable, increasing, or decreasing irradiation. By optimizing the perturbation scheme for the different cases, it can achieve faster tracking during irradiation change and more accuracy at steady state. The proposed optimized dP-P&O method has been implemented and compared to the basic dP-P&O and the classical P&O algorithm. The experimental results show that both algorithms perform clearly better than the classical P&O algorithm, providing accurate tracking even in very fast changing irradiation conditions.

References

[1] [s.n], "Trends in photovoltaic applications. Survey report of selected IEA countries between 1992 and 2005," Int. Energy Agency, Paris, France, Rep. IEA-PVPS Task 1 T1-15:2006, 2006. [Online]. Available: http://www.iea-pvps.org/products/download/rep1_15.pdf

[2] D. Hohm and M. Ropp, "Comparative study of maximum power point tracking algorithms using an experimental, programmable, maximum power point tracking test," in *Proc. 28th IEEE Conf. Rec. Photovoltaic Spec.*, 2000, pp. 1699–1702.

[3] W. Xiao and W. Dunford, "A modified adaptive hill climbing MPPT method for photovoltaic power systems," in *Proc. 35th IEEE Annu. PESC*, 2004, vol. 3, pp. 1957–1963.

[4] C. W. Tan, T. Green, and C. Hernandez-Aramburo, "An improved maximum power point tracking algorithm with current-mode control for photovoltaic applications," in *Proc. Int. Conf. PEDS*, 2006, vol. 1, pp. 489–494.

[5] L. Egiziano, N. Femia, D. Granozio, G. Petrone, G. Spagnuolo, and M. Vitelli, "Photovoltaic inverters with Perturb & Observe MPPT technique and one-cycle control," in *Proc. IEEE Int. Symp. Circuits Syst.*, 2006, pp. 3718–3721.

[6] T. Shimizu, O. Hashimoto, and G. Kimura, "A novel high-performance utility-interactive photovoltaic inverter system," *IEEE Trans. Power Electron.*, vol. 18, no. 2, pp. 704–711, Mar. 2003.

[7] J.-H. Park, J.-Y. Ahn, B.-H. Cho, and G.-J. Yu, "Dual-module-based maximum power point tracking control of photovoltaic systems," *IEEE Trans. Ind. Electron.*, vol. 53, no. 4, pp. 1036–1047, Jun. 2006.

[8] J.-M. Kwon, K.-H. Nam, and B.-H. Kwon, "Photovoltaic power conditioning system with line connection," *IEEE Trans. Ind. Electron.*, vol. 53, no. 4, pp. 1048–1054, Jun. 2006.

[9] W. Xiao, W. G. Dunford, P. R. Palmer, and A. Capel, "Application of centered differentiation and steepest descent to maximum power point tracking," *IEEE Trans. Ind. Electron.*, vol. 54, no. 5, pp. 2539–2549, Oct. 2007.

[10] I.-S. Kim, M.-B. Kim, and M.-J. Youn, "New maximum power point tracker using sliding-mode observer for estimation of solar array current in the grid-connected photovoltaic system," *IEEE Trans. Ind. Electron.*, vol. 53, no. 4, pp. 1027–1035, Jun. 2006.

[11] E. Roman, R. Alonso, P. Ibanez, S. Elorduizapatarietxe, and D. Goitia, "Intelligent PV module for grid-connected PV systems," *IEEE Trans. Ind. Electron.*, vol. 53, no. 4, pp. 1066–1073, Jun. 2006.

[12] C. Hua and C. Shen, "Comparative study of peak power tracking techniques for solar storage system," in *Proc. 13th Annu. APEC*, 1998, vol. 2, pp. 679–685.

[13] N. Femia, G. Petrone, G. Spagnuolo, and M. Vitelli, "Perturb and Observe MPPT technique robustness improved," in *Proc. IEEE Int. Symp. Ind. Electron.*, 2004, vol. 2, pp. 845–850.

[14] D. Sera, T. Kerekes, R. Teodorescu, and F. Blaabjerg, "Improved MPPT method for rapidly changing environmental conditions," in *Proc. IEEE Int. Symp. Ind. Electron.*, 2006, vol. 2, pp. 1420–1425.

[15] V. V. R. Scarpa, G. Spiazzi, S. Buso, "Low complexity MPPT technique exploiting the effect of the PV cell series resistance," in *Proc. 23rd Annu. IEEE APEC Expo.*, Feb. 24–28, 2008, pp. 1958–1964. [Online]. Available: http://ieeexplore.ieee.org/iel5/4510696/4522647/04522996.pdf

[16] N. Femia, G. Petrone, G. Spagnuolo, and M. Vitelli, "Optimization of Perturb and Observe maximum power point tracking method," *IEEE Trans. Power Electron.*, vol. 20, no. 4, pp. 963–973, Jul. 2005.

[17] W. Xiao, W. Dunford, and A. Capel, "A novel modeling method for photovoltaic cells," in *Proc. 35th IEEE Annu. PESC*, 2004, vol. 3, pp. 1950–1956.

[18] G. Walker, "Evaluating MPPT converter topologies using a Matlab PV model," *J. Electr. Electron. Eng. Aust.*, vol. 21, no. 1, pp. 49–55, 2001.

[19] A. Wagner, "Peak-power and internal series resistance measurement under natural ambient conditions," in *Proc. EuroSun*, Copenhagen, Denmark, 2000.

[20] J. Bishop, "Computer simulation of the effect of electrical mismatches in photovoltaic cell interconnection circuits," *Sol. Cells*, vol. 25, pp. 73–89, 1988.

Dezso Sera (S'05) received the B.S. degree in electrical engineering and the M.S. degree in drives automation with energetic performances from the Technical University of Cluj-Napoca, Cluj-Napoca, Romania, in 2001 and 2002, respectively. In 2005, he received the M.Sc. degree in power electronics and drives from Aalborg University, Aalborg East, Denmark, where he is currently working toward the Ph.D. degree in the Institute of Energy Technology.

His interests include modeling, diagnostics, maximum power point tracking, and control of grid-connected photovoltaic systems.

Remus Teodorescu (S'94–M'99–SM'02) received the Dipl.Ing. degree in electrical engineering from the Polytechnical University of Bucharest, Bucharest, Romania, in 1989 and the Ph.D. degree in power electronics from the University of Galati, Galati, Romania, in 1994.

Since 1998, he has been with the Power Electronics Section, Institute of Energy Technology, Aalborg University, Aalborg East, Denmark, where he is currently a Full Professor. He has more than 120 papers published, one book, and three patents (pending). His areas of interest are design and control of power converters used in renewable energy systems, distributed generation of mainly wind power and photovoltaics, computer simulations, and digital control implementation. He is the Founder and Coordinator of the Green Power Laboratory, Aalborg University, where he is focusing on the development and test of grid converters for renewable energy systems. He is also the Coordinator of the Vestas Power Program.

Dr. Teodorescu is the corecipient of the Technical Committee Prize Paper Awards at the IEEE Industry Applications Society (IAS) Annual Meeting 1998 and the Third-ABB Prize Paper Award at the IEEE Optim 2002. He is an Associate Editor for the IEEE POWER ELECTRONICS LETTERS and the Chair of the IEEE Danish Joint Industrial Electronics Society/Power Electronics Society/IAS Chapter.

Jochen Hantschel, photograph and biography not available at the time of publication.

Michael Knoll was born in 1981 in Friedrichshafen, Germany. He received the Dipl. Engineer degree in electrical engineering from the University of Ulm, Ulm, Germany, in 2007. In his diploma thesis, he designed, assembled, and tested a new topology for a high-efficiency grid converter for photovoltaic applications.

After his studies, he was with the Software Department, REFU-Elektronik, where he worked on the implementation of the maximum power point tracker in a grid-converter. Currently, he is with the Development Department, Daimler AG, Stuttgart, Germany.